IEEE Photonics Journal
An IEEE Photonics Society Publication

Performance Analysis of Dual-Hop RF-UWOC Systems

Volume 12, Number 2, April 2020

Hongjiang Lei, *Senior Member, IEEE*
Yiyao Zhang
Ki-Hong Park, *Member, IEEE*
Imran Shafique Ansari, *Member, IEEE*
Gaofeng Pan, *Senior Member, IEEE*
Mohamed-Slim Alouini, *Fellow, IEEE*

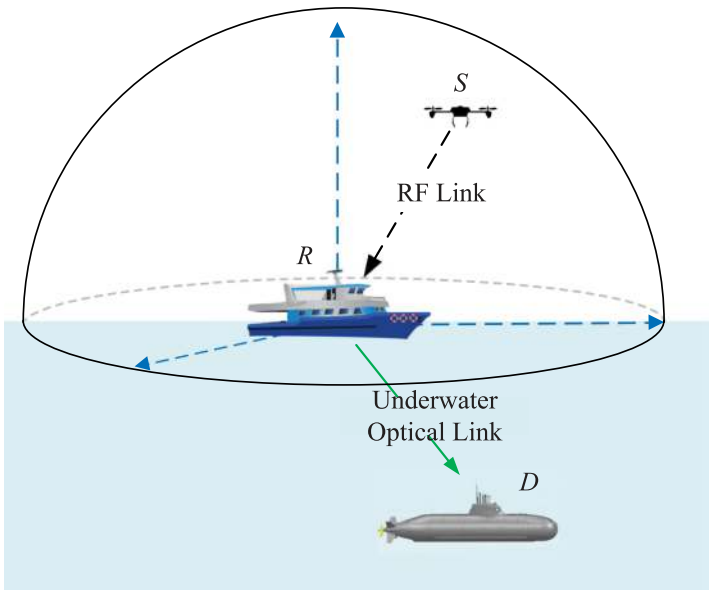

DOI: 10.1109/JPHOT.2020.2983016

Performance Analysis of Dual-Hop RF-UWOC Systems

Hongjiang Lei [1,2] ***Senior Member, IEEE***, **Yiyao Zhang** [1]
Ki-Hong Park [3] ***Member, IEEE***,
Imran Shafique Ansari [4] ***Member, IEEE***,
Gaofeng Pan [5] ***Senior Member, IEEE***,
and Mohamed-Slim Alouini [3] ***Fellow, IEEE***

[1]School of Communication and Information Engineering & Chongqing Key Laboratory of Ubiquitous Sensing and Networking, Chongqing University of Posts and Telecommunications, Chongqing 400065, China
[2]Shaanxi Key Laboratory of Information Communication Network and Security, Xi'an University of Posts and Telecommunications, Xi'an 710121, China
[3]CEMSE Division, King Abdullah University of Science and Technology (KAUST), Thuwal 23955-6900, Saudi Arabia
[4]James Watt School of Engineering, Glasgow G12 8QQ, U.K.
[5]School of Information and Electronics Engineering, Beijing Institute of Technology, Beijing 100081, China

DOI:10.1109/JPHOT.2020.2983016

Manuscript received February 29, 2020; accepted March 21, 2020. Date of publication March 30, 2020; date of current version April 16, 2020. This work was supported in part by the National Natural Science Foundation of China under Grant 61971080, in part by the Chongqing Natural Science Foundation Project under Grant cstc2019jcyj-msxm1354, and in part by the Open Fund of the Shaanxi Key Laboratory of Information Communication Network and Security under Grant ICNS201807. Corresponding author: Hongjiang Lei (e-mail: leihj@cqupt.edu.cn).

Abstract: In this paper, we analyze the performance of a dual-hop radio frequency-underwater wireless optical communication (RF-UWOC) transmission systems wherein the RF and UWOC links experience Nakagami-*m* fading and the mixture Exponential-Generalized Gamma fading, respectively. The location of *S* is uniformly distributed in the space of the hemisphere where the relay is located in the center of the hemisphere. The effect of bubbles level, temperature gradient, water types, and detection techniques are considered. We derive closed-form expressions for outage probability (OP) and average bit error rate (ABER) for both fixed and variable gain relaying schemes with different detection techniques. Furthermore, by utilizing the expansion of Meijer's *G*-function and Fox's *H*-function, the closed-form expressions for the asymptotic OP and ABER are derived when the average signal-to-noise ratio of both links tends to infinity. The analytical results are verified by Monte Carlo simulation results. Our results demonstrate that the diversity order of the dual-hop RF-UWOC systems depends on the RF fading parameter and detection technology of the UWOC link.

Index Terms: Dual-hop radio frequency-underwater wireless optical communication systems, Nakagami-*m* fading, mixture Exponential-Generalized Gamma fading, outage probability, average bit error rate.

1. Introduction

In recent years, underwater wireless communication (UWC) systems have gained great interest recently as it realizes many potential applications for both civil and military purposes, such as,

ecological monitoring, climate recording, and military surveillance. Three types of carriers were utilized in UWC systems to transmit signals, which are radio-frequency (RF) waves, acoustic waves, and optical waves. The extremely severe attenuation at high frequencies limits the propagation range, which make RF-based UWC systems unrealistic [1]. Although the acoustic-based UWC system solves the propagation range of RF-based UWC systems, lower propagation celerity in salt water causes serious delays and latency [2]. Compared with the acoustic and RF approach, underwater wireless optical communication (UWOC) technology can obtain highest data rate and energy efficiency, the lowest link delay and implementation costs. Additionally, low latency and low energy consumption make UWOC widely accepted as an appropriate communication solution in the underwater medium [1], [2].

In order to provide reference and guidance for the application, the performance of the UWOC systems was investigated in many works, such as [3]–[5]. The effect of temperature change on turbulence-induced fading of UWOC channels was investigated in [3] and their results have shown that the weak temperature-induced turbulence can be modeled by Generalized Gamma distribution. Zedini *et al.* proposed that the mixture Exponential-Gamma model can efficiently characterize the fluctuations of UWOC channels from weak to strong turbulence conditions for fresh and salty waters in [4]. In their journal version [5], the influence of air bubbles, temperature, and salinity gradient was investigated, the mixture Exponential-Generalized Gamma (EGG) distribution model was proposed to describe air bubbles and temperature-induced irradiance fluctuations for both weak and strong turbulence conditions in fresh and salty waters. Then, a unified performance analysis of UWOC systems was given while both intensity modulation/direct detection (IM/DD) and heterodyne detection techniques (HD) were considered. The closed-form expressions for the outage probability (OP), average bit error rate (ABER), and ergodic capacity were derived. Recently, the dual-hop RF-UWOC systems have received widespread attention since RF and UWOC technologies have been deployed together to achieve both advantages simultaneously [1]. The analytical expression for ABER of the dual-hop RF-UWOC system was derived for various binary modulation techniques in [6]. The secrecy performance of the dual-hop RF-UWOC systems was investigated in [7] and the closed-form expression for the intercept probability for the fixed-gain relaying (FGR) scheme was derived. In their journal version [8], the authors derived the closed-form expressions for the average secrecy capacity and intercept probability under FGR or variable gain relaying (VGR) schemes.

To explore how air bubbles, temperature, and salinity gradient factors affect the performance, a dual-hop RF-UWOC system is considered, where a source (S) with random location communicates with an underwater destination with the help of an amplify-and-forward (AF) relay. The main contributions of this work are listed as follows:

- The performance of the dual-hop RF-UWOC systems is investigated wherein the RF and UWOC links are modeled by Nakagami-m and EGG distributions, respectively. The closed-form expressions for OP and ABER under both the VGR and FGR schemes are derived for different detection techniques.
- To obtain more insights, we also investigate the asymptotic performance of the RF-UWOC systems when average signal-to-noise ratio (SNR) approaches infinity. The closed-form expressions for asymptotic OP and ABER are derived by utilizing the expansion of Meijer's G-function and Fox's H-function. The asymptotic results demonstrate that the diversity order of the dual-hop systems depends on the RF fading parameter and detection technology of the UWOC link.
- The accuracy of the analytical results is validated by Monte-Carlo simulations. The results show that when the bubbles level and the temperature gradient gets lower, the whole system works better. Relative to VGR scheme, FGR scheme demonstrates better performance. The performance of HD technique outperforms that of IM/DD.
- Relative to [8], wherein the secrecy performance was investigated and the expressions for average secrecy capacity and intercept probability were derived, respectively, we assume a different system model where S is uniformly distributed in the space of the hemisphere (V), and R is located in the center of the hemisphere. Furthermore, the asymptotic analysis of OP and ABER is performed and the diversity orders are derived in this work.

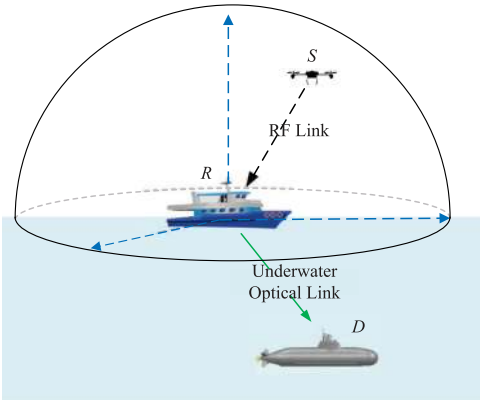

Fig. 1. System model of a dual-hop RF-UWOC systems that consists of a source (S), a relay (R), and a desired destination (D).

The remainder of this work is organized as follows. In Section 2, the dual-hop RF-UWOC system model and the statistical characteristics of each link are presented. The expressions of OP, ABER and its asymptotic results are derived in Section 3. Monte-Carlo simulation and numerical results are presented in Section 4. Finally, we conclude the work in Section 5.

2. Channel and System Model

As shown in Fig. 1, a dual-hop RF-UWOC system is considered. The information (such as commands or weather messages) is transmitted by source node (S) to the destination (D) through an AF relay (R). It is assumed that S is suspended in the air, but its location is uncertain for the given time. It is assumed that the RF link between the transmitter and the relay, and the UWOC link between the relay and the destination are relatively static, the doppler effect is ignored in this work. The results in this work also fit for those scenarios wherein the transmitter moves on the lower velocity and the Doppler effect due to the source mobility is assumed to be perfectly compensated. Then, we assumed that S with a single RF antenna is uniformly distributed in the space of the hemisphere (V), where R is located in the center of the hemisphere. The AF relay, R, has a RF antenna from one side and a single photo-aperture transmitter from the other side, while D is equipped with a single photo detector. The RF and UWOC links are assumed to experience quasi-static Nakagami-m and EGG distribution fading models, respectively.

2.1 The SNR of RF Link

The instantaneous SNR at R is expressed as

$$\gamma_{SR} = \rho_0 d_{SR}^{-\alpha} G_{SR}, \tag{1}$$

where $\rho_0 = P_S/\sigma^2$, P_S denotes the transmit power, σ^2 signifies the noise power at R, d_{SR} denotes the distance between S and R, α is the path loss exponent, and $G_{SR} = |g_{SR}|^2$ is the channel power gain. It is assumed that the RF link experiences Nakagami-m fading model, whose probability density function (PDF) is given by [9]

$$f_{G_{SR}}(x) = \frac{\Omega^m}{\Gamma(m)} x^{m-1} e^{-\Omega x}, \tag{2}$$

where $\Omega = m/\bar{\gamma}_1$. The parameter m signifies the level of fading. Nakagami-m includes Rayleigh ($m = 1$) and the one-sided Gaussian distribution ($m = 0.5$) as special cases. When $m \to \infty$, Nakagami-m fading channel converges to a non-fading AWGN channel. $\bar{\gamma}_1$ signifies average channel power gain of the RF link, and $\Gamma(\cdot)$ is Gamma function [10, (8.310.1)].

The CDF of d_{SR} is expressed as [11]

$$F_{d_{SR}}(d) = \begin{cases} \frac{d^3}{H^3}, & 0 \le d \le H, \\ 1, & d > H, \end{cases} \tag{3}$$

where H is the radius of hemisphere. Then, the cumulative distribution function (CDF) of $\frac{d_{SR}^{\alpha}}{\rho_0}$ is obtained as

$$\begin{aligned} F_{\frac{d_{SR}^{\alpha}}{\rho_0}}(y) &= \Pr\left\{\frac{d_{SR}^{\alpha}}{\rho_0} \le y\right\} \\ &= \begin{cases} \frac{(\rho_0 y)^{\varpi}}{H^3}, & 0 < y \le \frac{H^{\alpha}}{\rho_0}, \\ 1, & y \ge \frac{H^{\alpha}}{\rho_0}, \end{cases} \end{aligned} \tag{4}$$

where $\varpi = 3/\alpha$. Then we obtain

$$f_{\frac{d_{SR}^{\alpha}}{\rho_0}}(y) = \frac{3\rho_0^{\varpi}}{\alpha H^3} y^{\varpi - 1}, 0 < y < \frac{H^{\alpha}}{\rho_0}. \tag{5}$$

Based on (1), (2), utilizing [10, (3.351.1),(9.31.5)] and [12, (8.4.16.1)], the PDF of γ_{SR} is obtained as

$$\begin{aligned} f_{\gamma_{SR}}(\gamma) &= \int_0^{\infty} t f_{G_{SR}}(\gamma t) f_{\frac{d_{SR}^{\alpha}}{\rho_0}}(t) dt \\ &= \frac{3\rho_0^{\varpi}\Omega^{-\varpi}}{\alpha H^3 \Gamma(m)} \gamma^{-\varpi-1} \Upsilon(\varpi + m, \eta\gamma), \end{aligned} \tag{6}$$

where $\eta = \Omega H^{\alpha}/\rho_0$ and $\Upsilon(\cdot,\cdot)$ is low incomplete Gamma function [10, (8.350.1)]. Utilizing [12, (8.4.16.1)] and [13, (26)], we obtain

$$\begin{aligned} F_{\gamma_{SR}}(\gamma) &= \int_0^{\gamma} f_{\gamma_{SR}}(t) dt \\ &= \frac{3\rho_0^{\varpi}\Omega^{-\varpi}}{\alpha H^3 \Gamma(m)} \int_0^{\gamma} t^{-\varpi-1} G_{1,2}^{1,1}\left[\eta t \Big|_{\varpi+m,0}^{1}\right] dt \\ &= \varphi G_{2,3}^{1,2}\left[\eta\gamma \Big|_{m,-\varpi,0}^{1,1-\varpi}\right], \end{aligned} \tag{7}$$

where $\varphi = 3/[\alpha\Gamma(m)]$ and $G_{p,q}^{m,n}[\cdot]$ is the Meijer's G-function as defined by [10, (9.301)]. When $\bar{\gamma}_1 \to \infty$, $\Omega \to 0$, by using $\Upsilon(a,x) \overset{x\to 0^+}{\sim} (x^a/a)$, we obtain the asymptotic PDF and CDF as

$$f_{\gamma_{SR}}^{\infty}(\gamma) = \Phi_1 \gamma^{m-1}, \tag{8}$$

$$F_{\gamma_{SR}}^{\infty}(\gamma) = \frac{\Phi_1}{m}\gamma^m, \tag{9}$$

respectively, where $\Phi_1 = \frac{3\Omega^m H^{\alpha\varpi+\alpha m-3}}{\alpha\rho_0^m \Gamma(m)(\varpi+m)}$. It should be noted that m can be any real number in this work.

2.2 The SNR of UWOC Link

The instantaneous SNR at R is expressed as [5]

$$\gamma_{RD} = \mu_r I^r, \tag{10}$$

where r is the parameter specifying the type of detection technique (i.e. $r = 1$ for HD and $r = 2$ for IM/DD), $\mu_1 = \bar{\gamma}_2$, $\mu_2 = \frac{\bar{\gamma}_2}{2\omega\lambda^2 + b^2(1-\omega)\Gamma(a+2/c)/\Gamma(a)}$, $\bar{\gamma}_2$ signifies the average SNR of the UWOC link, ω is the mixture weight of the distributions, $0 < \omega < 1$, λ is the parameter associated with the Exponential distribution, a, b, and c are the parameters of the Generalized Gamma distribution. The value for ω, λ, a, b, and c are provided in [5, Tabels I and II].

The CDF and PDF of the UWOC link is given as [5]

$$F_{\gamma_{RD}}(\gamma) = \sum_{i=1}^{2} A_i G_{1,2}^{1,1}\left[B_i \gamma^{C_i} \Big|_{D_i,0}^{1}\right], \tag{11}$$

$$f_{\gamma_{RD}}(\gamma) = \sum_{i=1}^{2} E_i \gamma^{-1} G_{0,1}^{1,0}\left[B_i \gamma^{C_i} \Big|_{D_i}^{-}\right], \tag{12}$$

where $A_1 = \omega$, $B_1 = 1/[\lambda {\mu_r}^{(1/r)}]$, $C_1 = 1/r$, $D_1 = 1$, $E_1 = \omega/r$, $A_2 = [1-\omega]/\Gamma(a)$, $B_2 = 1/[b^c {\mu_r}^{(c/r)}]$, $C_2 = c/r$, $D_2 = a$, and $E_2 = [c(1-\omega)]/[r\Gamma(a)]$. The asymptotic SOP when $\bar{\gamma}_2 \to \infty$ is expressed as [5]

$$F_{\gamma_{RD}}^{\infty}(\gamma) = \sum_{i=1}^{2} F_i \gamma^{C_i D_i}, \tag{13}$$

where $F_1 = [\omega {\mu_r}^{(C_1 D_1)}]/\lambda$ and $F_2 = [(1-\omega)(b^r \mu_r)^{(C_2 D_2)}]/\Gamma(a+1)$.

3. Performance Analysis

3.1 Outage Probability Analysis With Variable-Gain Relay

In this case, the received SNR at D is approximately achieved by [14]

$$\gamma_{eq}^{\mathrm{V}} \cong \min(\gamma_{SR}, \gamma_{RD}), \tag{14}$$

Based on (7), (11), and (14), we obtain P_{out} in this case as

$$\begin{aligned} P_{out}^{\mathrm{V}} &= \Pr\left\{\gamma_{eq}^{V} < \gamma_{th}\right\} \\ &= F_{\gamma_{SR}}(\gamma_{th}) + F_{\gamma_{RD}}(\gamma_{th}) - F_{\gamma_{SR}}(\gamma_{th}) F_{\gamma_{RD}}(\gamma_{th}). \end{aligned} \tag{15}$$

It is assumed that $\bar{\gamma}_1 = \bar{\gamma}_2 = \bar{\gamma} \to \infty$, $P_{out}^{\mathrm{V},\infty}$ is rewritten as

$$P_{out}^{\mathrm{V},\infty} = \Psi_1 \bar{\gamma}^{-m} \gamma_{th}^{m} + \sum_{i=1}^{2} K_i \bar{\gamma}^{-C_i D_i} \gamma_{th}^{C_i D_i}, \tag{16}$$

where $\Psi_1 = \frac{3 m^{m-1} H^{\alpha\varpi+\alpha m-3}}{\alpha \rho_0^{m} \Gamma(m)(\varpi+m)}$, $K_1 = \omega B_1$, and $K_2 = (1-\omega)(B_2)^a/\Gamma(a+1)$. Then, the diversity order in this case is obtained as

$$G_d^{\mathrm{V}} = -\lim_{\bar{\gamma}\to\infty} \frac{\ln P_{out}^{\infty}}{\ln \bar{\gamma}} = \min(m, C_i D_i). \tag{17}$$

Based on Table 2, it is observed that $ac > 1$. Then the diversity order is expressed as

$$G_d^{\mathrm{OP,V}} = \min\left(m, \frac{1}{r}\right). \tag{18}$$

Remark 1:

From (18), one can observe that the diversity order of the dual-hop system with VGR depends on the detection techniques of UWOC link and the fading parameter of RF link.

3.2 Outage Probability Analysis With Fixed-Gain Relay

The received SNR at D with this scheme is given as [14]

$$\gamma_{eq}^{\mathrm{F}} = \frac{\gamma_{SR}\gamma_{RD}}{\gamma_{RD} + \Lambda}, \tag{19}$$

where Λ stands for the fixed relay gain [14]. The P_{out}^{F} is obtained as

$$P_{out}^{\mathrm{F}} = F_{\gamma_{SR}}(\gamma_{th}) + \left(1 - F_{\gamma_{SR}}(\gamma_{th})\right)\mu \sum_{i=1}^{2} A_i \phi_i, \tag{20}$$

where

$$\mu = \frac{3\Omega H^{\alpha(\varpi+1)-3}}{\rho_0 \Gamma(m)\alpha},\ \phi_i = \gamma_{th} H_{1,0;3,1;2,2}^{0,1;1,2;1,1}\left[\begin{matrix}(2,-C_i,1)\\ -\end{matrix}\middle|\begin{matrix}(1-D_i,1),(0,C_i),(1,1)\\ (0,1)\end{matrix}\middle|\begin{matrix}(2-m,1),(2+\varpi,1)\\ (1+\varpi,1),(1,1)\end{matrix}\middle|\vartheta_i,\ \frac{1}{\eta\gamma_{th}}\right],$$

$\vartheta_i = (B_i \Lambda^{C_i})^{-1}$, and $H_{p_1,q_1:p_2,q_2:p_3,q_3}^{m_1,n_1:m_2,n_2:m_3,n_3}[\cdot]$ is the Extended Generalized Bivariate Fox's H-function (EGBFHF), as defined by [15, (1.2)].

Proof:

See Appendix A. ■

Remark 2:

Eq. (20) is easy to understand, in which the first item denotes the OP of the first link and the second item signifies the joint OP of the dual-hop systems when the first link does not occur outage.

When $\bar{\gamma}_1 = \bar{\gamma}_2 = \bar{\gamma} \to \infty$, $P_{out}^{\mathrm{F},\infty}$ is obtained as

$$P_{out}^{\mathrm{F},\infty} = F_{\gamma_{SR}}^{\infty}(\gamma_{th}) + \left(1 - F_{\gamma_{SR}}^{\infty}(\gamma_{th})\right)\mu \sum_{i=1}^{2} A_i \phi_i^{\infty}, \tag{21}$$

where ϕ_i^{∞} is given by (47) and (48). The diversity order of the dual-hop RF-UWOC systems with FGR scheme is obtained as

$$G_d^{\mathrm{OP,F}} = \min\left(m, \frac{2}{r}\right). \tag{22}$$

Proof:

See Appendix B. ■

Remark 3:

From (22), one can observe that the diversity order of the OP for the dual-hop system with VGR depends on the detection techniques of UWOC link and the fading parameter of RF link.

3.3 Average Bit Error Rate With Variable-Gain Relay

A unified expression for the ABER for a variety of modulation schemes can be given as [5]

$$\bar{P}_e = \frac{\delta}{2\Gamma(p)} \sum_{k=1}^{n} \int_0^{\infty} \Gamma(p,\ q_k\gamma) f_{\gamma}(\gamma)\, d\gamma, \tag{23}$$

where n, δ, p, and q_k depend on the adopted modulation technique and the type of detection (i.e IM/DD or HD), as summarized in Table 1.[1] The end-to-end ABER can be given as

$$\bar{P}_e^{\mathrm{V}} = \bar{P}_e^{SR} + \bar{P}_e^{RD} - 2\bar{P}_e^{SR}\bar{P}_e^{RD}, \tag{24}$$

[1]As we knew, OOK is on-off keying where the symbol is mapped into zero amplitude (or intensity in IM/DD) or positive amplitude. So it can be viewed as a biased BPSK. For example, we assume modulate in a BPSK scheme i.e., mapping into $+1$ or -1. After shifting this constellation by $+1$, it will be OOK, which means that OOK has a power penalty due to this bias. Therefore, it doesn't need to use OOK in HD, while suffering from this power penalty. Contrarily, BPSK, M-PSK, and M-QAM schemes are not taken into consideration in HD.

TABLE 1
Parameters for Different Modulations [5]

Modulation	δ	p	q_k	n	Detection Type
OOK	1	0.5	0.25	1	IM/DD
BPSK	1	0.5	1	1	HD
M-PSK	$\frac{2}{\max(\log_2(M),2)}$	0.5	$\sin^2\left(\frac{(2k-1)\pi}{M}\right)$	$\max\left(\frac{M}{4},1\right)$	HD
M-QAM	$\frac{4}{\log_2(M)}\left(1-\frac{1}{\sqrt{M}}\right)$	0.5	$\frac{3(2k-1)^2}{2(M-1)}$	$\frac{\sqrt{M}}{2}$	HD

where $\bar{P}_e^{SR}$ and $\bar{P}_e^{RD}$ are the ABER for the RF and UWOC links, respectively.

Substituting (6) into (23), utilizing [12, (8.4.16.1)] and [13, (21)], we obtain

$$\begin{aligned}\bar{P}_e^{SR} &= \frac{\delta}{2\Gamma(p)}\sum_{k=1}^{n}\int_0^{\infty}\Gamma\left(p,\ q_k\gamma\right)f_{\gamma_{SR}}\left(\gamma\right)d\gamma \\ &= \frac{\delta\mu}{2\Gamma(p)}\sum_{k=1}^{n}\int_0^{\infty}G_{1,2}^{2,0}\left[q_k\gamma\left|\begin{matrix}1\\0,p\end{matrix}\right.\right]G_{1,2}^{1,1}\left[\eta\gamma\left|\begin{matrix}-\varpi\\m-1,-\varpi-1\end{matrix}\right.\right]d\gamma \\ &= \frac{\delta\mu}{2\Gamma(p)}\sum_{k=1}^{n}q_k^{-1}G_{3,3}^{1,3}\left[\frac{\eta}{q_k}\left|\begin{matrix}-\varpi,0,-p\\m-1,-1,-\varpi-1\end{matrix}\right.\right].\end{aligned} \tag{25}$$

Substituting (12) into (23), utilizing [12, (8.4.16.1)], [16, (2.9.1)], and [16, (2.8.11)], we obtain

$$\begin{aligned}\bar{P}_e^{RD} &= \frac{\delta}{2\Gamma(p)}\sum_{k=1}^{n}\int_0^{\infty}\Gamma\left(p,\ q_k\gamma\right)f_{\gamma_{RD}}\left(\gamma\right)d\gamma \\ &= \frac{\delta}{2\Gamma(p)}\sum_{k=1}^{n}\sum_{i=1}^{2}E_i\int_0^{\infty}\gamma^{-1}H_{1,2}^{2,0}\left[q_k\gamma\left|\begin{matrix}(1,1)\\(0,1),(p,1)\end{matrix}\right.\right]H_{0,1}^{1,0}\left[B_i\gamma^{C_i}\left|\begin{matrix}-\\(D_i,1)\end{matrix}\right.\right]d\gamma \\ &= \frac{\delta}{2\Gamma(p)}\sum_{k=1}^{n}\sum_{i=1}^{2}E_iH_{2,2}^{1,2}\left[B_i\left|\begin{matrix}(1,C_i),(1-p,C_i)\\(D_i,1),(0,C_i)\end{matrix}\right.\right].\end{aligned} \tag{26}$$

Based on (9) and (13), the asymptotic ABER of RF link and UWOC link is obtained as

$$\begin{aligned}\bar{P}_e^{SR,\infty} &= \frac{\Phi_1\delta}{2\Gamma(p)}\sum_{k=1}^{n}\int_0^{\infty}\gamma^{m-1}\Gamma\left(p,\ q_k\gamma\right)d\gamma \\ &= \frac{\Psi_1\delta\Gamma\left(p+m\right)}{2\Gamma(p)q_k^m}\bar{\gamma}^{-m},\end{aligned} \tag{27}$$

$$\bar{P}_e^{RD,\infty} = \frac{\delta}{2\Gamma(p)}\sum_{k=1}^{n}\sum_{i=1}^{2}J_i\bar{\gamma}^{-C_iD_i}, \tag{28}$$

respectively, where $J_1=\omega B_1\Gamma(p+\frac{1}{r})q_k^{-(1/r)}$ and $J_2=\frac{(1-\omega)}{\Gamma(a+1)}B_2^a\Gamma(p+\frac{ac}{r})q_k^{-([ac]/c)}$. Then, the diversity order of ABER for VGR is obtained as

$$G_d^{\mathrm{ABER,V}} = \min\left(m,\frac{1}{r}\right) = G_d^{\mathrm{OP,V}}. \tag{29}$$

Remark 4:

One can observe that the diversity order of ABER for VGR is dependent on the detection technology and is independent of modulation schemes and equal to the diversity order of OP for VGR.

3.4 Average Bit Error Rate With Fixed-Gain Relay

The ABER in this case is rewritten as

$$\bar{P}_e^{\mathrm{F}} = \frac{\delta q_k^p}{2\Gamma(p)} \sum_{k=1}^{n} \int_0^{\infty} \gamma^{p-1} e^{-q_k \gamma} F_{\gamma_{eq}^{\mathrm{F}}}(\gamma)\, d\gamma. \tag{30}$$

Then, substituting (20) into (30), the ABER with FGR is obtained as

$$\bar{P}_e^{\mathrm{F}} = \bar{P}_e^{SR} + \frac{\mu\delta q_k^p}{2\Gamma(p)} \sum_{k=1}^{n} \sum_{i=1}^{2} A_i \varphi_i - \frac{\mu\delta q_k^p}{2\Gamma(p)} \sum_{k=1}^{n} \sum_{i=1}^{2} A_i \psi_i, \tag{31}$$

where

$$\varphi_i = q_k^{-p-1} H_{1,0;3,1;2,3}^{0,1;1,2;2,1} \left[\begin{matrix} (2,-C_i,1) \\ - \end{matrix} \middle| \begin{matrix} (1-D_i,1),(0,C_i),(0,1) \\ (0,1) \end{matrix} \middle| \begin{matrix} (2-m,1),(2+\varpi,1) \\ (1+\varpi,1),(p+1,1),(1,1) \end{matrix} \middle| \vartheta_i, \frac{q_k}{\eta} \right], \tag{32}$$

and

$$\psi_i = \frac{\varphi m! \eta^{1+p}}{q_k^{2p+2}} H_{1,0;3,1;4,4}^{0,1;1,2;1,3} \left[\begin{matrix} (2,-C_i,1) \\ - \end{matrix} \middle| \begin{matrix} (1-D_i,1),(0,C_i),(1,1) \\ (0,1) \end{matrix} \middle| \begin{matrix} (2+p,1),(2+p-\varpi,1),(2-m,1),(2+\varpi,1) \\ (1+\varpi,1),(1-\varpi+p,1),(1+p,1),(1,1) \end{matrix} \middle| \vartheta_i, \frac{q_k^2}{\eta^2} \right]. \tag{33}$$

Proof:

See Appendix C. ■

When $\bar{\gamma}_1 = \bar{\gamma}_2 = \bar{\gamma} \to \infty$, with the same method presented in Appendix B, the asymptotic ABER with FGR is obtained as

$$P_e^{\mathrm{F},\infty} \approx \bar{P}_e^{SR,\infty} + \frac{\mu\delta q_k^p}{4\pi^4\Gamma(p)} \sum_{k=1}^{n} \sum_{i=1}^{2} A_i \varphi_i^{\infty}, \tag{34}$$

where $\bar{P}_e^{SR,\infty}$ is given in (27),

$$\varphi_i^{\infty} = \begin{cases} \dfrac{\Gamma(p+1)(\varpi+1)(\ln(\Theta) - \ln(\Gamma(p+1))) + \varpi + 2}{\eta (q_k)^p \Theta (\varpi+1)^2}, & m=1, i=1, r=1 \\ \dfrac{\Gamma(0.5)\Gamma(p+0.5)}{\eta (q_k)^p \Theta (\varpi+0.5)}, & m=1, i=1, r=2 \\ \dfrac{\Gamma(a-\tau)\Gamma(p+1)}{\eta (q_k)^p (1+\varpi) \Theta^{\tau}}, & m=1, i=2 \\ \dfrac{q_k \Gamma(p+\tilde{r})}{\eta\Theta} \dfrac{\ln\left(\dfrac{\Gamma(p+\tilde{r})}{\Theta}\right)(\varpi+\tilde{r}) + (\varpi+2\tilde{r})}{(\varpi+\tilde{r})^2}, & m=0.5, i=1, r=2 \\ \dfrac{\Gamma(m-\tilde{r})\Gamma(p+\tilde{r})}{(q_k)^p \eta (\varpi+\tilde{r}) \Theta}, & m \neq 1, m \neq 0.5, i=1 \\ \dfrac{\Gamma(p+m)\Gamma(a-\tau)\Lambda(B_2)^{\tau}}{(q_k)^{p+m}(\varpi+m)\eta^{1-m}}, & m \neq 1, i=2 \end{cases}, \tag{35}$$

$\Theta_i = \frac{1}{B_i}(\frac{q_k}{\eta\Lambda})^{C_i}$, $\tilde{r} = \frac{1}{r}$, and $\tau = \frac{r}{c}$. Similarly, $G_{i,d}^{\varphi}$, which denotes the diversity order of $\sum_{i=1}^{2} A_i \varphi_i^{\infty}$, is obtained as

$$G_{i,d}^{\varphi} = \frac{2}{r} - 1. \tag{36}$$

Thus, the diversity order of ABER for FGR is obtained as

$$G_d^{\mathrm{ABER,F}} = \min\left(m, \frac{2}{r}\right) = G_d^{\mathrm{OP,F}}. \tag{37}$$

TABLE 2
Parameters of the EGG Distribution [5]

$\hbar\,(L/\min)$	$\ell\,(^{\circ}C.cm^{-1})$	ω	λ	a	b	c
2.4	0.05	0.2130	0.3291	1.4299	1.1817	17.1984
2.4	0.10	0.2108	0.2694	0.6020	1.2795	21.1611
2.7	0.05	0.4589	0.3449	1.0421	1.5768	35.9424
4.7	0.10	0.4539	0.2744	0.3008	1.7053	54.1422

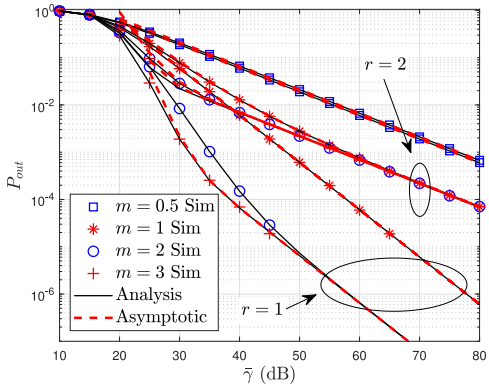

Fig. 2. OP for VGR versus $\bar{\gamma}$ with $\hbar = 2.4$ and $\ell = 0.05$.

Remark 5:

One can observe that the diversity order of ABER for FGR is independent of modulation schemes and equal to that of OP for FGR.

4. Numerical Results

Simulation results are provided in this section to confirm the accuracy of the analyzed results. The main parameters are set as $\alpha = 2$, $\gamma_{th} = 1.3$, and $\Lambda = 1.1$. 'Sim' in the following figures denote simulation results. The parameters of UWOC link are given in Table 2, shown at the top of this page, where $\hbar(L/\min)$ and $\ell(^{\circ}\mathrm{C}\cdot\mathrm{cm}^{-1})$ signify the level of the air bubbles and temperature gradient, respectively. One can observe that the simulation results perfect match with the analytical results, confirming the accuracy of our results.

The OP of the considered dual-hop RF-UWOC system with VGR or FGR under the same turbulence conditions is presented in Figs. 2–4 as a function of the varying environmental conditions, fading parameters of RF link, and detection technique adopted over UWOC link. For the VGR scheme, the bottleneck of the dual-hop systems is the UWOC link. More specifically, the OP with $r = 1$ outperforms that with $r = 2$, which means HD technique can obtain better performance compared with IM/DD technology, as presented in Fig. 2. The fading of RF link almost shows no effect in the case wherein the IM/DD technology is utilized over UWOC link. For such scenarios with HD technology, weak RF fading also does not influence the OP of the dual-hop systems in a larger-γ region. Moreover, the diversity order for the OP under VGR depends on the adopted detection technique and the RF fading.

As depicted in Fig. 3, one can observe that the performance of the considered dual-hop system under the FGR scheme is limited by the first hop, the RF link. In detail, for those scenarios with strong fading ($m \leq 1$), the equal OP is obtained for different r, in which the effect of the adopted detection technologies on OP is weak. The detection technique is the main parameter for those scenarios when $m > 1$. The diversity order under FGR is also verified as presented in Fig. 3. When the fading of the RF link and the adopted detection technique over the UWOC link are the same, the outage performance of the considered dual-hop system under FGR is superior to that under

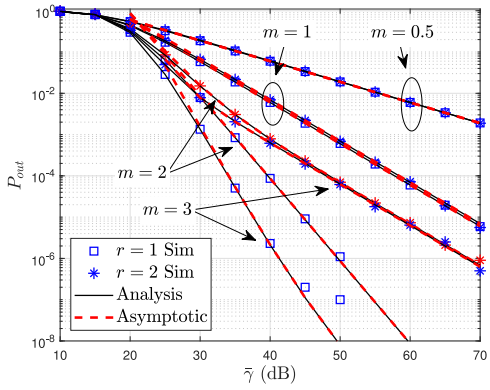

Fig. 3. OP for FGR versus $\bar{\gamma}$ with $\hbar = 2.4$ and $\ell = 0.05$.

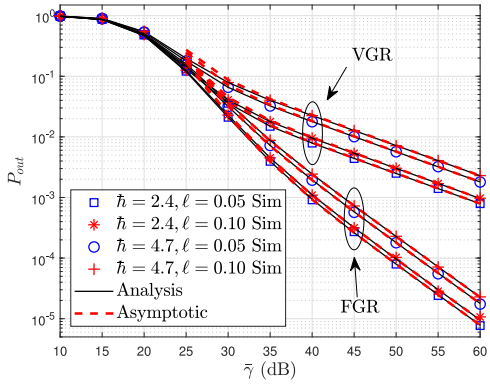

Fig. 4. OP versus $\bar{\gamma}$ with varying environmental parameters, $m = 2$, and $r = 2$.

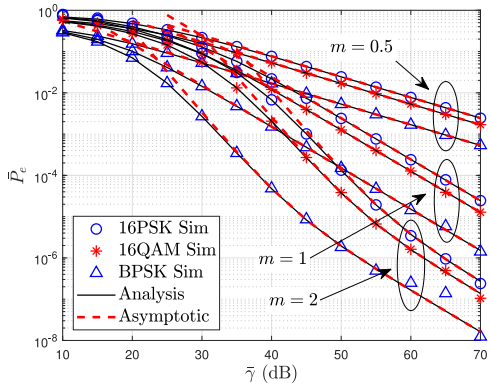

Fig. 5. ABER for VGR versus $\bar{\gamma}$ with $\hbar = 2.4$ and $\ell = 0.05$.

VGR, which is testified as presented in Fig. 4. Moreover, the effect of the level of the air bubbles is more severe than that of the temperature gradient. One can observe that the outage performance of the considered dual-hop system becomes worse when the level of the air bubbles and/or the temperature gradient is higher.

Figs. 5–7 demonstrate the ABER of the considered dual-hop RF-UWOC system with VGR or FGR under different modulations. We can observe from Figs. 5 and 6 that BPSK modulation

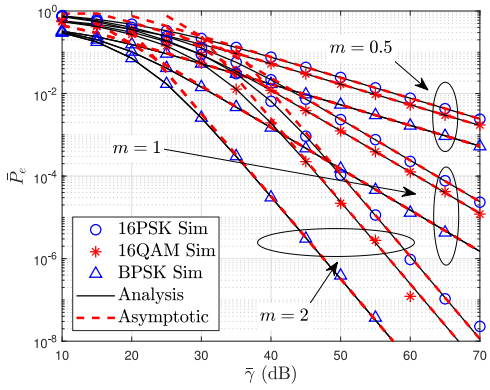

Fig. 6. ABER for FGR versus $\bar{\gamma}$ with $\hbar = 2.4$ and $\ell = 0.05$.

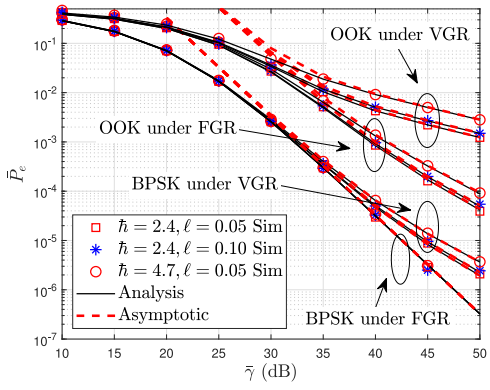

Fig. 7. ABER versus $\bar{\gamma}$ with varying environmental parameters and $m = 2$.

outperforms 16QAM, which is better than that of 16PSK. The ABER with $m > 1$ outperforms that with $m \leq 1$ while a larger m implies that the fading of the RF link is weak. Furthermore, one can observe that the diversity order of ABER is independent of the employed modulation schemes. From Fig. 7, it is observed that the ABER with FGR is superior to that with the VGR scheme. The level of the air bubbles and temperature gradient exhibits no influence on the diversity order of ABER. Moreover, one can observe that the ABER of the dual-hop system becomes worse when the level of the air bubbles and/or the temperature gradient is higher, which is similar as the observations from Fig. 4. This is because higher value of the scintillation index leads to stronger turbulence.

5. Conclusion

In this work, we analyzed the performance of dual-hop RF-UWOC systems. The closed-form expressions of the analytical and asymptotic OP and ABER for both the VGR and FGR under different detection techniques were derived and validated through Monte-Carlo simulations results. Our results demonstrate that the performance with lower bubbles level and temperature gradient outperforms that with higher bubbles level and temperature gradient. Relative to VGR scheme, FGR achieve better performance. The performance of HD technique outperforms of with IM/DD. The asymptotic results illustrated that the diversity order of the dual-hop systems depends on the RF fading parameter and the detection technology adopted over UWOC link.

Appendix A

Based on (19), the OP for FGR is obtained as

$$\begin{aligned} P_{out}^{\mathrm{F}} &= \Pr\left\{\frac{\gamma_{SR}\gamma_{RD}}{\gamma_{RD}+\Lambda} < \gamma_{th}\right\} \\ &= \Pr\left\{\left(\gamma_{SR}-\gamma_{th}\right)\gamma_{RD} < \Lambda\gamma_{th}\right\} \\ &= \Pr\left\{\gamma_{SR} < \gamma_{th}\right\} + \Pr\left\{\gamma_{RD} < \frac{\Lambda\gamma_{th}}{\gamma_{SR}-\gamma_{th}}, \gamma_{SR} > \gamma_{th}\right\} \\ &= \Pr\left\{\gamma_{SR} < \gamma_{th}\right\} + \Pr\left\{\gamma_{RD} < \frac{\Lambda\gamma_{th}}{\gamma_{SR}-\gamma_{th}} | \gamma_{SR} > \gamma_{th}\right\} \Pr\left\{\gamma_{SR} > \gamma_{th}\right\} \\ &= F_{\gamma_{SR}}\left(\gamma_{th}\right) + \left(\int_{\gamma_{th}}^{+\infty} F_{\gamma_{RD}}\left(\frac{\Lambda\gamma_{th}}{t-\gamma_{th}}\right) f_{\gamma_{SR}}(t)dt\right)\left(1-F_{\gamma_{SR}}\left(\gamma_{th}\right)\right) \\ &= F_{\gamma_{SR}}\left(\gamma_{th}\right) + \left(1-F_{\gamma_{SR}}\left(\gamma_{th}\right)\right)\mu\sum_{i=1}^{2} A_i\phi_i, \end{aligned} \tag{38}$$

where $\mu = \frac{3\Omega H^{\alpha(\varpi+1)-3}}{\rho_0\Gamma(m)\alpha}$ and $\phi_i = \int_{\gamma_{th}}^{\infty} G_{1,2}^{1,1}[B_i(\frac{\Lambda\gamma_{th}}{t-\gamma_{th}})^{C_i}|_{D_i,0}^{1}]G_{1,2}^{1,1}[\eta t|_{m-1,-\varpi-1}^{-\varpi}]dt$.

Let $x = t-\gamma_{th}$, making use of [10, (9.301),(3.194.3),(8.384.1)] in turn, we obtain

$$\begin{aligned} \phi_i &= \int_0^{\infty} G_{1,2}^{1,1}\left[B_i\left(\frac{\Lambda\gamma_{th}}{x}\right)^{C_i}|_{D_i,0}^{1}\right] G_{1,2}^{1,1}\left[\eta\left(x+\gamma_{th}\right)|_{m-1,-\varpi-1}^{-\varpi}\right] dx \\ &= \frac{1}{(2\pi i)^2}\int_{\mathcal{L}_1}\int_{\mathcal{L}_2} \frac{\Gamma(-s)\Gamma(D_i+s)}{\Gamma(1-s)B_i^s}\frac{\Gamma(1+\varpi-t)\Gamma(m-1+t)}{\Gamma(2+\varpi-t)\eta^t} \\ &\quad\times\int_0^{\infty}\left(\frac{x}{\Lambda\gamma_{th}}\right)^{sC_i}\frac{1}{(x+\gamma_{th})^t}dxdtds \\ &= \frac{\gamma_{th}}{(2\pi i)^2}\int_{\mathcal{L}_1}\int_{\mathcal{L}_2}\Gamma(t-sC_i-1)\frac{\Gamma(1+\varpi-t)\Gamma(m-1+t)}{\Gamma(2+\varpi-t)\Gamma(t)} \\ &\quad\times\frac{\Gamma(-s)\Gamma(D_i+s)\Gamma(sC_i+1)}{\Gamma(1-s)}\frac{1}{(\eta\gamma_{th})^t}\vartheta_i^s dtds, \end{aligned} \tag{39}$$

where $\mathcal{L}_1$ and $\mathcal{L}_2$ are the s-plane and the t-plane contours, respectively. Then, by utilizing [17, (1.1)], we obtained the closed-form expression for ϕ_i.

Appendix B

According to [18], [19], expansions of the univariate and bivariate Meijer's G-function or Fox's H-functions can be derived by evaluating the residue of the corresponding integrands at the closest poles to the contour. More specifically, the Fox's H-function is defined as

$$H_{p,q}^{m,n}\left(x\left|\begin{matrix}(a_1,\alpha_1),\ldots,(a_p,\alpha_p)\\(b_1,\beta_1),\ldots,(b_q,\beta_q)\end{matrix}\right.\right) = \frac{1}{2\pi i}\int_C x^{-s}h(s)ds, \tag{40}$$

where $h(s) = \frac{\prod_{j=1}^{m}\Gamma(b_j+\beta_j s)\prod_{i=1}^{n}\Gamma(1-a_i-\alpha_i s)}{\prod_{i=n+1}^{p}\Gamma(a_i+\alpha_i s)\prod_{j=m+1}^{q}\Gamma(1-b_j-\beta_j s)}$. The asymptotic result can be approximated by

$$\begin{aligned} \lim_{x\to y} H_{p,q}^{m,n}\left(x\left|\begin{matrix}(a_1,\alpha_1),\ldots,(a_p,\alpha_p)\\(b_1,\beta_1),\ldots,(b_q,\beta_q)\end{matrix}\right.\right) &= \lim_{s\to\xi}\frac{1}{(u-1)!}\frac{d^{u-1}}{ds^{u-1}}\left[(s-\xi)^u h(s)x^{-s}\right] \\ &= \lim_{s\to\xi}\frac{1}{(u-1)!}\frac{d^{u-1}}{ds^{k-1}}\left[\frac{\Gamma^u(s-\xi+1)}{\Gamma^u(s-\xi)}h(s)x^{-s}\right], \end{aligned} \tag{41}$$

where

$$\xi = \begin{cases} \max_{j=1:m}\left(-\frac{b_j}{\beta_j}\right), & y=\infty \\ \min_{i=1:n}\left(\frac{1-a_i}{\alpha_i}\right), & y=0 \end{cases}$$

denotes the maximum (minimum) pole on the left (right) with arbitrary order u.

We rewrite (39) as

$$\phi_1 = \frac{\gamma_{th}}{2\pi i}\int_{L_1} \frac{\Gamma(-s)\,\Gamma(D_i+s)\,\Gamma(sC_i+1)}{\Gamma(1-s)\left(B_i\Lambda^{C_i}\right)^s}\left(\frac{1}{2\pi i}\int_{L_2} g_1(t)dt\right)ds, \tag{42}$$

where

$$g_1(t) = \begin{cases} \frac{\Gamma(t-sC_i-1)\Gamma(1+\varpi-t)}{\Gamma(2+\varpi-t)(\eta\gamma_{th})^t}, & m=1 \\ \frac{\Gamma(t-sC_i-1)\Gamma(m-1+t)\Gamma(1+\varpi-t)}{\Gamma(2+\varpi-t)\Gamma(t)(\eta\gamma_{th})^t}, & m\neq 1 \end{cases}. \tag{43}$$

When $m=1$, the integral over L_2 can be approximated by

$$\begin{aligned} \frac{1}{2\pi i}\int_{L_2} g_1(t)dt &\approx \lim_{t\to sC_i+1}(t-sC_i-1)\,g_1(t) \\ &= \frac{\Gamma(\varpi-sC_i)}{\Gamma(1+\varpi-sC_i)(\eta\gamma_{th})^{sC_i+1}}. \end{aligned} \tag{44}$$

Substituting (44) into (42), we have

$$\phi_1 = \frac{1}{2\eta\pi i}\int_{L_1} \frac{\Gamma(-s)\,\Gamma(D_i+s)\,\Gamma(sC_i+1)\,\Gamma(\varpi-sC_i)}{\Gamma(1-s)\,\Gamma(1+\varpi-sC_i)}\Xi_i^s ds, \tag{45}$$

where $\Xi_i = (B_i(\eta\Lambda\gamma_{th})^{C_i})^{-1}$. For the integral over L_1 with $m=1$, there are two poles on the left side, which are $s=-D_i$ and $s=-\frac{1}{C_i}$, respectively. The maximum pole is given as

$$\max\left\{-D_i, -\frac{1}{C_i}\right\} = \begin{cases} -D_i = -\frac{1}{C_i}, & i=1, r=1 \\ -D_i, & i=1, r=2 \\ -\frac{1}{C_i}, & i=2 \end{cases}. \tag{46}$$

Utilizing (41), and by recalling that $\frac{d(\Gamma(s))}{ds} = \Gamma(s)\Psi^{(0)}(s)$, $\Psi^{(0)}(s) = \ln(\Gamma(s))$, $\frac{d(a^s)}{ds} = a^s\ln(a)$, after some algebraic manipulations, ϕ_i with $m=1$ is approximated by

$$\phi_1^{\infty} = \begin{cases} \frac{(\ln(\Xi_1))(\varpi+1)+\varpi+2}{\eta\Xi_1(\varpi+1)^2}, & i=1, r=1 \\ \frac{\Gamma(0.5)}{\eta(\varpi+0.5)\Xi_1}, & i=1, r=2 \\ \frac{\Gamma\left(a-\frac{r}{c}\right)}{\eta(\varpi+1)}\Xi_2{}^{-\frac{r}{c}}, & i=2 \end{cases}. \tag{47}$$

When $m\neq 1$, there are two poles for the integral over L_2, $t=sC_i+1$ and $t=1-m$, which are the selected poles for $i=1$ and $i=2$, respectively. With the same method as (44)–(45), we obtain

$$\phi_1^{\infty} = \begin{cases} \frac{\ln(\Xi_1)(\varpi+0.5)-(\varpi+1)}{\eta\Xi_1(\varpi+0.5)^2}, & i=1, mr=1 \\ \Gamma\left(m-\frac{1}{r}\right)\left(\eta\Xi_1\left(\varpi+\frac{1}{r}\right)\right)^{-1}, & i=1, mr\neq 1 \\ \frac{\Gamma\left(a-\frac{r}{c}\right)\vartheta_2{}^{\frac{r}{c}}}{\eta(\varpi+m)(\eta\gamma_{th})^{-m}}, & i=2 \end{cases}. \tag{48}$$

Because of $\Omega\sim\bar{\gamma}^{-1}$, $\mu\sim\bar{\gamma}^{-1}$, $\Phi_1\sim\bar{\gamma}^{-m}$, $B_1\sim\bar{\gamma}^{-\frac{1}{r}}$, $B_2\sim\bar{\gamma}^{-\frac{c}{r}}$, $\eta\sim\bar{\gamma}^{-1}$, the diversity order in this case is obtained as

$$G_d^{\mathrm{OP,F}} = -\lim_{\bar{\gamma}\to\infty}\frac{\ln P_{out}^{\mathrm{F},\infty}}{\ln\bar{\gamma}} = \min\left(m, 1+\min\left\{G_{i,d}^{\phi}\right\}\right), \tag{49}$$

where $G_{i,d}^{\phi}$ signifies the diversity of $\sum_{i=1}^{2} A_i \phi_i^{\infty}$. Based on (47) and (48), we obtain

$$G_{i,d}^{\phi} = \begin{cases} 0.5, & m = 0.5 \\ 0, & m = 1 \\ \min\left\{\frac{2}{r} - 1, m\right\} & \text{others} \end{cases}. \tag{50}$$

Thus, we have (22).

Appendix C

Based on (39), utilizing [10, (3.194.3), (8.384.1), (3.326.2)], we obtain

$$\begin{aligned} \varphi_i &= \frac{1}{(2\pi i)^2} \int_{L_1} \int_{L_2} \frac{\Gamma(-s)\,\Gamma(D_i + s)}{\Gamma(1-s)\,B_i^s} \int_0^{\infty} \gamma^{p-1} e^{-q_k \gamma} \int_0^{\infty} (x+\gamma)^{-t} \left(\frac{x}{\Lambda\gamma}\right)^{sC_i} dx d\gamma \\ &\quad \times \frac{\Gamma(1+\varpi-t)\,\Gamma(m-1+t)}{\Gamma(2+\varpi-t)\,\eta^t} dt ds \\ &= \frac{(q_k)^{-p-1}}{(2\pi i)^2} \int_{L_1} \int_{L_2} \Gamma(t - sC_i - 1) \frac{\Gamma(-s)\,\Gamma(sC_i+1)\,\Gamma(D_i+s)}{\Gamma(1-s)\left(\Lambda^{C_i} B_i\right)^s} \\ &\quad \times \frac{\Gamma(1+\varpi-t)\,\Gamma(m-1+t)\,\Gamma(p+1-t)}{\Gamma(2+\varpi-t)\,\Gamma(t)} \left(\frac{q_k}{\eta}\right)^t dt ds. \end{aligned} \tag{51}$$

Then, by utilizing [17, (1.1)], we obtain the closed-form expression for ϕ_2 as (32). With the same method, (33) is obtained.

References

[1] Z. Zeng, S. Fu, H. Zhang, Y. Dong, and J. Cheng, "A survey of underwater optical wireless communications," *IEEE Commun. Surv. Tut.*, vol. 19, no. 1, pp. 204–238, Jan.–Mar. 2017.

[2] E. Illi, F. E. Bouanani, and F. Ayoub, "A high accuracy solver for RTE in underwater optical communication path loss prediction," in *Proc. Int. Conf. Adv. Commun. Technologies Netw.*, Marrakech, Morocco, Apr. 2018, pp. 1–8.

[3] H. M. Oubei *et al.*, "Simple statistical channel model for weak temperature-induced turbulence in underwater wireless optical communication systems," *Opt. Lett.*, vol. 42, no. 13, pp. 2455–2458, Jul. 2017.

[4] E. Zedini, H. M. Oubei, A. Kammoun, M. Hamdi, B. S. Ooi, and M.-S. Alouini, "A new simple model for underwater wireless optical channels in the presence of air bubbles," in *Proc. IEEE Global Commun. Conf.*, Singapore, Dec. 2017, pp. 1–6.

[5] E. Zedini, H. M. Oubei, A. Kammoun, M. Hamdi, B. S. Ooi, and M.-S. Alouini, "Unified statistical channel model for turbulence-induced fading in underwater wireless optical communication systems," *IEEE Trans. Commun.* vol. 67, no. 4, pp. 2893–2907, Apr. 2019.

[6] S. Anees and R. Deka, "On the performance of DF based dual-hop mixed RF/UWOC system," in *Proc. IEEE 89th Veh. Technol. Conf.*, Kuala Lumpur, Malaysia, Apr. 2019, pp. 1–5.

[7] E. Illi, F. El Bouanani, D. B. da Costa, F. Ayoub, and U. S. Dias, "On the secrecy performance of mixed RF/UOW communication system," in *Proc. IEEE Global Commun. Conf.*, Abu Dhabi, UAE, Dec. 2018, pp. 1–6.

[8] E. Illi, F. E. Bouanani, D. B. d. Costa, F. Ayoub, and U. S. Dias, "Dual-hop mixed RF-UOW communication system: A PHY security analysis," *IEEE Access*, vol. 6, pp. 55345–55360, 2018.

[9] M. K. Simon and M.-S. Alouini, *Digital Communication over Fading Channels*, 2. Hoboken, NJ, USA: Wiley, 2005.

[10] I. Gradshteyn and I. Ryzhik, *Table of Integrals, Series and Products*, 7th ed. San Diego, CA, USA: Academic, 2007.

[11] J. Ye, C. Zhang, H. Lei, G. Pan, and Z. Ding, "Secure UAV-to-UAV systems with spatially random UAVs," *IEEE Wireless Commun. Lett.*, vol. 8, no. 2, pp. 564–567, Apr. 2019.

[12] A. P. Prudnikov, Y. A. Brychkov, and O. I. Marichev, *Integrals and Series: Vol. 3: More Special Functions*. Boca Raton, FL, USA: CRC Press, 1992.

[13] V. S. Adamchik and O. I. Marichev, "The algorithm for calculating integrals of hypergeometric type functions and its realization in REDUCE system," in *Proc. Int. Symp. Symbolic Algebraic Comput.*, Tokyo, Japan, Aug. 1990, pp. 212–224.

[14] M. O. Hasna and M.-S. Alouini, "A performance study of dual-hop transmissions with fixed gain relays," *IEEE Trans. Wireless Commun.*, vol. 3, no. 6, pp. 1963–1968, Nov. 2004.

[15] A. M. Mathai, R. K. Saxena, and H. J. Haubold, *The H-Function: Theory and Applications*. Berlin, Germany: Springer, 2009.

[16] A. A. Kilbas and M. Saigo, *H-Transforms: Theory and Applications*. Boca Raton, FL, USA: CRC Press, 2004.
[17] P. K. Mittal and K. C. Gupta, "An integral involving generalized function of two variables," *Proc. Indian Academy Sci. - Section A*, vol. 75, no. 3, pp. 117–123, Mar. 1972.
[18] H. Chergui, M. Benjillali, and S. Saoudi, "Performance analysis of project-and-forward relaying in mixed MIMO-pinhole and Rayleigh dual-hop channel," *IEEE Commun. Lett.*, vol. 20, no. 3, pp. 610–613, Mar. 2016.
[19] L. Kong, G. Kaddoum, and H. Chergui, "On physical layer security over Fox's *H*-function wiretap fading channels," *IEEE Trans. Veh. Technol.*, vol. 68, no. 7, pp. 6608–6621, Jul. 2019.